Realizing Integral Field Spectroscopy in the Far-Infrared

Leslie W. Looney[1], Walfried Raab, Albrecht Poglitsch, Norbert Geis

Max-Planck-Institut für extraterrestrische Physik (MPE), Garching, Germany

ABSTRACT

The optical design of an integral field spectrometer for far-infrared observations, the Far-Infrared Field-Imaging Line Spectrometer (FIFI LS), is presented. The instrument will fly onboard the joint NASA/DLR airborne observatory SOFIA, observing in two nearly independent wavelength channels simultaneously: a Blue channel (40-105 microns) and a Red channel (105-210 microns). To achieve instantaneous integral field spectroscopy for the first time in the far-infrared, a novel reflective image slicer system is utilized that slices the 5×5 pixel, 2-dimensional field of view into a pseudo long-slit of 25×1 pixels. The slicer assembly consists of 3 sets of 5 mirrors that have optical power, enabling a compact design. After the sky field has been optically re-arranged to the pseudo slit, the image is spectrally dispersed in a standard Littrow mounted reflective grating spectrometer. The practical concerns for the optical design in the far-infrared and in particular the significant effect of diffraction in the entire optical system is discussed.

Subject headings: instrumentation: spectrographs, techniques: image processing, techniques: spectroscopic

1. Introduction

Modern astronomical research relies heavily upon spectroscopic analysis of extended source emission (e.g. disks of galaxies to disks of young stellar objects) wherein both spectral (radial velocity) and spatial (the two dimensions of the image field) information, so called 3-dimensional imaging, is required to best probe the physical conditions of the source. However incoherent detectors are currently limited to 2-dimensional arrays that require practical spectrometers to preferentially choose two of the 3-dimensional quantities: for a long slit spectrometer a range of 1 spatial and 1 spectral coordinates at a given spatial coordinate

[1]New Address: University of Illinois Urbana-Champaign Email: lwl@uiuc.edu

and for a Fabry-Perot spectrometer a range of 2 spatial coordinates at a given wavelength coordinate. In point-like or simple geometry sources, a single slit spectrum may be sufficient for the desired science objectives, but for more complicated sources, one must spatially scan the single long-slit spectrometer across the extended source, or spectrally scan a Fabry-Perot spectrometer across the wavelength coordinates of interest.

In the two above implementations of extended source spectroscopy, there are some major disadvantages. The most obvious of which is that only 2 dimensions of the needed 3 dimensional data cube can be observed at a single time. In order to obtain the entire data cube, either the remaining spatial coordinate for a long-slit spectrometer or the next wavelength channel for a Fabry-Perot spectrometer needs to be observed, both requiring more observing time. This adds a layer of difficulty; in the time taken to change the pointing or scan the Fabry-Perot, the observing conditions (e.g. seeing or pointing errors) or instrumental responsivity may change, adding systematic noise to the data cube.

Instantaneous imaging of a 3-D data cube with two spatial dimensions and one spectral dimension has been successful with three types of systems: fiber optic feeds, lenslet arrays, or reflective image slicers. The first astronomical application of integral field spectroscopy was performed with optical fiber bundles that were arranged into a pseudo-slit, feeding a long-slit spectrometer (Vanderriest 1980). Fiber optic feed instruments are being used successfully in a number of optical and near-infrared instruments (e.g. INTEGRAL and SMIRFS; Arribas et al. 1998; Haynes et al. 1999). The second widely used technique is the application of a microlens, or lenslet, array that is placed in the focal plane of the telescope (Courtès 1982). Each lens in the array forms a micro-pupil that is dispersed onto available regions on the detector (e.g. TIGER and SAURON; Bacon et al. 1995, 2001). Also lenslets can be added to fiber systems to increase the filling factor of the focal plane. In the final case, reflective image slicer mirrors effectively slice the the image plane into a number of individual slices that are re-arranged into a single pseudo-slit then dispersed with a traditional slit spectrometer (e.g. MPE3D and SPIFFI; Weitzel et al. 1996; Eisenhauer et al. 2000).

A separate technique that should be mentioned for obtaining the 3 dimensional data cube is a Fourier Transform Spectrometer (FTS). Although an FTS does not instantaneously image a spectral line, thus still having problems with changing observing conditions, it does sample the Fourier transform, or interferogram, of the spectrum via a Michelson type of interferometer. While it is an excellent choice for systems where the detector read-noise is the dominant source of noise, the multiplex spectral advantage can also be multiplex disadvantage in systems where the spectral fill factor of the observation is small (i.e. when the instrument spectral response is dominated by non-spectral line channels and noise is introduced into the sampled Fourier components). Because of this, an FTS concept is not

very efficient in the far-infrared where detectors are background noise limited and designs tend toward small spectral filling factors.

In all of the above cases, a 2 dimensional detector can be utilized to image the 3 dimensional data cube; however only the lenslets, fiber, and reflective image slicers can perform instantaneous spectroscopy of extended sources. In addition, only with the advent of large format, far-infrared photoconductor arrays (e.g. SIRTF; Heim et al. 1998), where one has enough low-noise pixels, can far-infrared integral field spectrometers be practical and useful. Indeed, in the longer wavelengths of the far-infrared these arrays have been difficult to produce (see Rosenthal et al. 2000), but now reasonable sized arrays (a requirement for integral field spectroscopy at these wavelengths) can be constructed (25×16; Hönle et al. 2004). In this paper, the first design for a far-infrared integral field spectrometer utilizing an image slicer technique, is presented– the Far-Infrared Field-Imaging Line Spectrometer (FIFI LS) instrument. Although FIFI LS will be the first far-infrared integral field spectrometer in operation, it is being designed simultaneously with a spaceborne instrument the Photodetector Array Camera and Spectrometer (PACS, see Poglitsch et al. 2003) onboard Herschel (expected launch in 2007, see Pilbratt 2003) that has a similar optical design.

The FIFI LS design is driven by the goal of maximizing observing efficiency, especially for nearby galaxies. Since the sensitivity of a well designed far-infrared instrument is limited by the thermal background of telescope and atmosphere, even for a stratospheric observatory, observing efficiency can only be increased by increasing the throughput of the spectrometer and the number of simultaneous (useful) data channels.

2. FIFI LS Instrument Overview

With the Stratospheric Observatory For Infrared Astronomy (SOFIA, e.g. Erickson 1995; Krabbe & Röser 1999), astronomers will soon (expected first light in late 2004) have access to unprecedented spatial resolution and sensitivity in the far-infrared that is completely inaccessible from the ground due to atmospheric water absorption. Building upon the success of the predecessor far-infrared instrument FIFI (Poglitsch et al. 1991), a Fabry-Perot spectrometer for the KAO (see Larson 1995), a successor instrument for SOFIA is being constructed: FIFI LS (also see Geis et al. 1998; Looney et al. 2000, 2003), which will capitalize upon the increase of sensitivity and spatial resolution that SOFIA offers to inject crucial data into many astrophysical questions.

FIFI LS was designed to optimize the observing efficency of far-infrared lines in extragalactic sources. In particular, the main scientific targets will include the detailed morpho-

logical studies of merging and interacting galaxies, heating and cooling processes of galaxies, star formation and the interstellar medium in the local galaxy and also under low-metallicity conditions, such as found in dwarf galaxies, active galactic nuclei and their environment, and large surveys of nearby galaxies. To reach the scientific goals, very high observing sensitivity and efficiency is essential. Primarily this is accomplished in three ways: (1) as mentioned in §1, a diffraction limited integral field concept allows simultaneous spectroscopic observations of a 2-dimensional field of view in the spectral line of interest, as well as the baseline of the spectral line; (2) for many of the science objectives, it is necessary to observe two far-infrared lines at once (e.g. [OI] at 63 μm and 146 μm), thus two nearly independent observing channels have incorporated– the so-called Blue (42-105 μm) and Red (105-210 μm) channels; and (3) for the science goals moderate resolution (R$\sim$2000) with large velocity coverage (always a trade-off) is obtained with a reflective grating spectrometer, allowing a well sampled spectrum in the spectral pixels. This set of design specifications will allow diffraction limited imaging of spectral lines with an instantaneous spectral coverage of $\sim$ 1500 km/s, reliably obtaining both the line and some baseline even for objects with high velocity dispersion.

Observing with an airborne telescope raises new and sometimes difficult problems. For example, for the optical system perhaps the biggest of these constraints is that the instrument is restricted in both size (the instruments must fit through the passenger door of the aircraft) and weight; the optical design requires a number of fold mirrors and some sacrifice in optical placement and performance to reduce the overall size and weight.

3. Optics

As discussed in §1, there are three basic types of integral field techniques. However in the far-infrared, practical spectrometers are limited to a reflective image slicer design: lenslet arrays or fiber that transmit with low loss and enough wavelength coverage do not exist. Indeed, overall refractive optics are not practical because of the limited wavelengths where diffractive materials operate and the lack of adequate anti-reflective coatings. On the other hand, aluminum, diamond turned or diamond milled, gold coated, reflective optics are available, have high quality, and have the same thermal expansion coefficient as an aluminum optical bench, providing more reliable alignment procedures.

The two simultaneous channels of FIFI LS, Blue and Red, operate as nearly independent spectrometers, merely sharing the same entrance optics and calibration sources. The optical overview, including the dual channels, is illustrated in block format (Figure 1), showing the major components of the design (entrance optics, slicer, spectrometer, exit optics) that are discussed in detail below. It is important to keep in mind that the main point of the FIFI

LS optics is to allow integral field spectroscopy, and in this section the critical design issues to achieve this in the far-infrared are addressed.

3.1. Entrance Optics

As shown schematically in Figure 1, the first optical component of the FIFI LS optical path is the infrared dichroic (also see Figure 2) that reflects the far-infrared beam into the cryostat and passes the near-infrared and visible beams to the attached CCD guider camera. The guider camera corrects for telescope pointing errors and drifts, and, in a telescope pupil imager mode, allows for accurate alignment between the SOFIA telescope and the far-infrared boresight. Following the dichroic, the entrance optics (Figure 2) are at liquid nitrogen temperature ($\sim$77 K) to reduce background thermal emission. The SOFIA telescope focuses the f/20 beam onto the first mirror of the FIFI LS K-mirror unit (Figure 2, E1). The three reflective surfaces (a large prism mirror E1 and E3 and a flat mirror E2) are held within a single unit that can be rotated around the central axis to compensate for sky rotation during integration. For example, if the K-mirror structure is turned via a geared stepper motor by an angle of α, the image field rotates about the center of field by 2α.

The second important function of the entrance optics is the proper refocusing of the diverging beam and scaling of the incoming SOFIA telescope image for the image slicer assembly using the ellipsoidal mirror (E5). The exact scaling will be discussed in §3.3. The calibration source, which also resides in the entrance section, is described in detail in §3.7. Finally, after some optical folding (the flat mirrors E4 and E6 that do not effect the image parity) the beam is injected through a Lyot stop into the helium cooled ($\sim$ 4 K) optical bench, wherein the optics for the slicers and the spectrometers are aligned.

3.2. Separation of Channels

After the beam enters the helium optical plate through the Lyot stop, the Blue and Red channels, 40-105 μm and 105-210 μm, respectively, are separated. This is accomplished via a multi-layer dichroic that is discussed further in §3.8. In order to allow some flexibility of observations, a cryogenic dichroic exchange mechanism is incorporated such that one of two dichroics can be placed into the beam, separating the Red and Blue channels at slightly different wavelengths (105 μm or 130 μm). One of the most useful design features of the FIFI LS optics is that from the dichroic onward, the two channels of the spectrometer are completely parallel and can be operated autonomously. Indeed, it is exactly like two separate

spectrometers from this point on.

It should also be noted that the optical designs of the Red and Blue channels are similar, but not exact copies of each other. Since the Blue channel has pixels that are a factor of 2 smaller on the sky to remain diffraction limited in both channels, the beam is magnified using elliptical mirrors (Figure 3; M1 and M2, with a folding mirror M3).

3.3. Slicer System

A first approach for integral field spectroscopy in the far-infrared would seem to be a scaling of the current near-infrared flat mirror designs (e.g. MPE 3D or SPIFFI; Weitzel et al. 1996; Eisenhauer et al. 2000). In these designs, a number of flat mirrors are arranged in a slightly tilted, area-filling, stack that directs the light to a second, flat mirror arrangement that then constructs a pseudo-slit. If the surfaces of the second mirror set are arranged along a hyperbolic surface, the pupil of the telescope is conserved and recombined (Weitzel et al. 1996; Tecza et al. 2000).

Unfortunately, the above designs are not practical in the far-infrared. The problem is that the conservation of energy dictates that the product of collecting area and accepted solid angle of the optics is directly proportional to the square of the wavelength ($A\Omega \sim \lambda^2$). So the essential optics in a flat-mirror design, both path length and physical size, would have to be enlarged by 100 times in each dimension with respect to the short wavelength flat-mirror instruments. This is prohibited in the application, due to the increased cost associated with very large diamond turned or milled optics and, of course, the instrument size limitation on SOFIA. However, as soon as mirrors with optical power are used in the slicer assembly design, allowing movement and resizing of pupils and foci almost at will, a much more compact system can be realized also in the far-infrared.

The major driving design goal of the imager slicer mirrors is to optically re-arrange, or slice, the 2 dimensional field of view into a 1 dimensional pseudo-slit that can easily be fed into any standard long slit spectrometer. Since this is done with only reflective elements, it adds difficulties into the design, particularly topological obstacles. With the available detectors for FIFI LS, a 5×5 pixel field of view for the image slicer is employed in both channels. Figure 4 shows a cartoon of how the input and output of a perfect optical slicer system should perform. The slicer re-arranges the field into a 29×1 pixel pseudo-slit– the 4 empty pixels are to reduce cross-talk between two pixels which are nonadjacent on the sky but adjacent on the pseudo-slit. Each pixel of the pseudo-slit is then dispersed onto 16 spectral pixels of the 25×16 pixel detector. Since far-infrared detectors are starved for pixels,

the detector columns for the four gaps are left empty. The slicer assembly is comprised of three sets of mirrors (similar in concept to Content 1997) in groups of 5 (corresponding to the 5×5 field) that influence the 5 rows of the 2 dimensional field. Only the Red channel slicer assembly is discussed as the concept applies to both channels.

First, the refocused field of view from the re-imaging optics (mirror E5, Figure 2) is folded via R1 and focused onto the slicer mirrors (Figure 5, R2a-R2e) a stack of 5 mirrors that are slightly tilted with respect to the center slice. In this paper, the nomenclature is that the term "slicer assembly" corresponds to the entire reflective image slicer system (the set of three times five mirrors that slice the 2-D field of view, see Figure 5) and the term "slicer mirror" refers to the first mirror in that assembly. As in the flat mirror designs (c.f. Weitzel et al. 1996), the basic premise is to redirect, or spatially fan-out, each row of the 2 dimensional field of view to the capture mirrors (Figure 5, R3a-R3e). As the beam is rather fast, the capture mirrors capture the pupil at a reasonable distance. The slicer mirrors are spherical mirrors that image the pupil onto the capture mirrors at a distance of ∼150 mm.

At this point, the field of view is dissected into 5 separate beams with distinct and separate pupils on the capture mirrors. The next step is to refocus the beams onto a 1-dimensional pseudo-slit and recombine the pupils such that a standard long-slit spectrometer design can be easily implemented. The capture mirrors, on-axis spherical biconics, are then angled to refocus the beam onto the last mirror in the set of 3 slicer assembly mirrors (the slit mirrors, Figure 5, R4a-R4e). The slit mirrors are on-axis spherical mirrors that are angled such that the 5 pupils are virtually re-imaged to a single pupil that originates ∼2000 mm away with an f/9.5 for the Red channel and an f/18.7 for the Blue channel.

One of the elegant features of this design is the uncoupling of the mirror functions. The slicer mirrors are field mirrors that produce an image of the pupil on the capture mirrors. The capture mirrors re-focus the beam to a focus on the slit mirrors, another set of field mirrors. Finally, the slit mirrors are reasonable for producing a virtual pupil that is inserted into the spectrometer via R5. With this isolation of function, the overall optimization, including the important geometry of the 15 mirrors, is performed one mirror set at a time, significantly reducing the overall complexity.

The pixel size of the instrument is set in the slicer system as the physical scale of the slicer mirror. The SOFIA telescope has the first zero of the Airy disk at approximately $9''$ and $16''$ for 90 μm and 160 μm, respectively. To Nyquist sample the beam for the Rayleigh condition requires $4.5''$ and $8''$ pixels. However, if the slicer mirrors were $4.5''$ or $8''$, the mirror would cut significantly into the Airy disk of the telescope, severely increasing the diffraction effects discussed in §4.2. As a compromise, to both minimize the effects of diffraction and allow for reconstruction of the telescope beam, the pixels are conservatively scaled to the

diffraction resolution, such that FIFI LS can still fully sample the beam by using a dithering observing technique. For this reason, the pixel size is set to 6″ and 12″ for the Blue and Red channels, respectively.

3.4. Spectrometer

The two 2-D fields of views, which are optically re-arranged into two 1-D pseudo-slits, are fed into two slightly offset Littrow mounted long-slit spectrometers for the Red and Blue channels (Figure 3). The focused beam of each pseudo-slit is collimated using two collimator mirrors which anamorphically image the pupil onto the grating; the same collimators are used to refocus the dispersed beam at the output. In an ideal Littrow mounted system, the input and output beams coincide, which is realistically impractical, so the FIFI LS design has a 28 mm separation between the two beams, or a 1.8° divergence. This results in a small loss of efficency. Since the dispersive aspect of the gratings occurs in only one direction, anamorphic collimation (a ratio of 2 and 3 for wavelengths of 90 μm and 160 μm respectively) is used to reduce the superfluous dimension of the grating and production costs. The anamorphic ratio was selected in such a way that the spectral resolution at 90 μm and 160 μm is roughly matched and that the diffraction gratings are near fully illuminated at the longest working wavelength, or the largest tilting angle.

Since the two wavelength channels suffer different magnification, the two channels have slightly differently designed spectrometers (Figure 6). In the Red channel, the first collimator mirror (R6), a parabolic cylindrical surface (flat mirror in one direction and an off-axis parabola in the other), collimates the beam in the x or cross-dispersion direction and the second mirror (R7), also a parabolic cylindrical surface, collimates the beam in the y or dispersion direction. Both mirrors are only active in one direction.

The collimator for the Blue channel is modified to illuminate fully the grating with the smaller pupil. The pathlengths of the two systems are nearly the same due to the geometric constraint of the cryostat, yet the pupil is enlarged considerably. In contrast to the Red channel, the first collimator mirror in the Blue channel (B6, flat in x and hyperbolic in y) expands significantly the y-direction while leaving the x-direction unchanged and the second mirror (B7, different parabolic surfaces in both directions) performs the final collimation in both the x and y-direction. Since both channels of the spectrometers are set-up in the nearly on-axis Littrow mounted scheme, the beam returns on nearly the same path, meaning that the beams get re-focused by using the same collimator mirrors; thus, any anamorphic distortion is undone by the second pass through the collimator system.

3.5. Diffraction Gratings

FIFI LS has two nearly independent optimized wavelength channels, which obviously need two separate gratings. The Red channel covers less than an octave of wavelength, and utilizes a grating operated in 1st grating order. The Blue channel uses 1st and 2nd order to fully cover its wavelength band. The observing wavelength is selected by physically tilting the grating, which changes the angle of the incident beam. In order to maximize the efficiency of the two gratings, the reflective grating profiles were extensively modeled using a program that fully solves the Maxwell equations for periodic boundary conditions, PCGrate 1E version 3.0 (Goray 1995). The gratings should have a maximum efficency at astronomical relevant wavelengths ($\sim$60 μm and $\sim$160 μm), yet the efficency should be relatively flat across the entire band of interest (redshifted galaxies need to be observed at offset wavelengths), and finally, the groove profile should be relatively easy to manufacture using a diamond tooled milling machine– generally triangular shaped. The final profile with the calculate efficency is shown in Figure 7 where the Red channel was optimized for only 1st order operation and the Blue channel for the combination of 1st and 2nd order.

3.6. Exit Optics

The exit optics are designed to accommodate the detector array characteristics and to minimize stray and background light. Due to the high reflectivity and low single-pass absorptivity of Ge:Ga, the pixels are placed in integrating cavities with small light-coupling holes and individual light cones, or light guides, that area-fill the focal plane. The exit optics and detectors are designed such that only light from the beam is injected into the cones– a last stage of stray light suppression. This is accomplished by making the focal plane a cylindrical surface (Hönle et al. 2004), rather than flat, with the individual light cones for each pixel pointing toward a small pupil (10 mm Ø) at a distance of 240 mm; light outside that pupil does not reach the detector.

In addition, the exit optics scale the dispersed light such that the spectra is Nyquist sampled. Three mirrors (B8, B9, and B10 in the Blue channel and R8, R9, and R10 in the Red channel, Figure 3) are used as an anamorphic camera, scaling the spectrum in the y-direction and the pixel size in the x-direction (Figure 15), with a common exit pupil as just described.

3.7. Calibration Optics

In addition to the optics train, there is a calibration source with respective injection optics, placed in the LN_2 section of the cryostat. The calibration of the absolute flux level is essential for astrophysical interpretation of the observations. The photometric calibration of the system is done by chopping between two known amplitudes to compare the difference, much as the observing compares the on-source and off-source sky positions. In practice, approximately every 20-30 minutes during observations, a flip-mirror inserts a calibration pupil into the entrance optics. This is an internal calibration process; the flip-mirror blocks any emission from the sky. The calibration pupil is produced by a single blackbody source near the temperature of the telescope that is coupled into a scattering sphere via a modulated entrance hole such that the pupil alternates between two intensities. This simulates chopping between two known amplitudes and is expected to allow, under similar background conditions, an absolute flux calibration that can be bootstrapped to about 20%. Similarly, a gas absorption cell can be placed in front of the instrument for initial wavelength calibration, with astronomical observations to confirm and interpolate the calibration.

3.8. Filters and Dichroic

Due to the spectral multiplexing nature of the design, it is of prime importance in FIFI LS to suppress scattered light from inside the instrument. Three filters are used in each channel to minimize the input radiation from outside the Helium cryostat, select out only the correct order of the grating, and minimize radiation into the superfluid Helium cryostat, respectively. The filters and dichroics (except the first dichroic) consist of a series of polypropylene foils that have thin periodic metal patterns applied to their surface via a photolithographic process, producing multi-layer interference filters (Ade 2003). By a suitable selection of metal geometry and refractive index of the substrate, any custom, or non-standard, filter combination can be produced. The advantages of this type of filter over Reststrahlen crystal filters, such as those employed in FIFI (Poglitsch et al. 1991), are that the wavelength coverage can be freely chosen, or "tuned" with high transmission, and that the filters have high stability and transmission reliability at cryogenic temperatures.

The blocking filters and dichroics used in FIFI LS are listed in Table 1. The filter at the Lyot stop, L2, suppresses short-wavelength ($\lambda < 40$ μm) radiation from entering the Helium cryostat. Because of overlapping grating diffraction orders an order selection filter is placed in front of the detector pupil. For the Blue channel, this filter is exchanged via a cryogenic mechanism whenever the grating order is changed– BO1 and BO2, or first and second order, respectively. These are bandpass filters, consisting of two filters– a high pass and a low

pass. For the Red channel, only one grating order is used and a filter can be permanently installed– RO1. Finally, the RAL and BAL filters are placed directly before the light cones of the Red and Blue detectors. This suppresses any stray light from other wavebands and minimize the background levels. To assure further that stray light and background light are minimized, RAL and BAL filters overlap the wavelength range of the fore-filters.

Two dichroic beam splitters are used in FIFI LS. The first one merely separates the far-infrared from the near-infrared and visible. Since the cutoff wavelength is around 2 μm, this can easily be composed of coated glass with simple gold layers, metal oxide-metal oxide coatings, or a thin layer of semiconductor material. The second dichroic beam splitter is placed immediately after the Lyot stop to separate the two channels. At the FIFI LS wavelengths, a hot-pressed plastic filter, as described above, does not work due to the bad reflecting quality. A modified design using an "air" gap (with layers stretched over a precision spacer ring to form the flat surfaces needed for reflection) is used for the switchable dichroics D1 and D2. However, this type of design is more difficult to handle due to the increased fragility and mechanical load sensitivity.

4. Optical Performance

In the following two subsections, the optical design of FIFI LS is analyzed. First, the popular ray tracing program Zemax version 10 from Focus Software is used to demonstrate how the slicer mirrors optically re-arrange the field and to calculate the system optical performance, including image spot size and Strehl ratios. Secondly, detailed diffraction analysis of the optics for the central slice is performed, in particular how diffraction affects the overall system spectral resolution using the scalar propagation method with the software package GLAD version 4.5 from Applied Optics Research. For simplicity, the FIFI LS optical system was transformed into on-axis lenses for the software diffraction analysis. Finally, a full vectorial diffraction analysis of the first two slicer mirrors is compared to the scalar solutions.

4.1. Ray Trace Analysis

To properly analyze the FIFI LS optical design, the SOFIA telescope optics is simulated such that it provides a diffraction limited image on the K-mirror (see §3.1). The telescope is a 2.5 m Nasmyth mounted f/20 telescope with an effective focal length of $\sim$50 m. After correction for field rotation by the K-mirror, the beam is re-imaged and the pupil is re-

established at the Lyot stop (helium work surface), as shown in Figure 8. It is important that this pupil has excellent quality, because the hole diameter in the optical plate is minimized to reduce background light into the helium cryostat.

As described in §3.3, the FIFI LS beam is focused onto the slicer mirrors (Figure 9), which create pupils on the capture mirrors (Figure 10). The capture mirrors then create the pseudo-slit focus (Figure 11) on the slit mirrors, which in turn re-create a virtual single pupil at the correct injection distance for the spectrometer (Figure 12). As shown in Figure 11, there is more curvature of the pseudo-slit in the Red channel than the Blue channel. This is a combined geometric effect of the differences in path length and angle of the beams in the slicer assembly. On several mirrors there are reflections out of the incoming beam plane that correspond to an optical rotation around the beam axis, or smile/frown of the pseudo-slit. Since the diffraction gratings are also tilted with respect to the off-axis spectrometer beams, they also display an output wavelength dependent slit curvature. Thus, the geometric effects of the slicer assembly rotation is designed to counteract the expected grating slit curvature at approximately 60 μm and 160 μm (see Figure 13). Note that in the Blue channel, the grating curvature is less pronounced so less curvature in the pseudo-slits is required.

The anamorphic magnification of the collimator mirrors creates a "pupil" on the grating (Figure 14). If diffraction in the system were negligible the number of lines illuminated would correspond directly to the system spectral resolution. After the spectrometer, the resulting dispersed beam is re-imaged onto the detector, again using anamorphic camera optics to scale the spectral pixels onto the detectors with Nyquist sampling. Figure 15 shows the final imaging at three wavelengths in the Red channel in the 1st grating order, and Figure. 16 and 17 show the final imaging of three wavelengths in the Blue channel in the 1st and 2nd grating orders. The Blue channel has a worse visual appearance and RMS spot size than the Red channel since it has been magnified by a factor of 2.

Overall, the optics provide an excellent correlation between the detector pixels and the pseudo-slits. The RMS of the final spot sizes are shown for the Red channel in Figure 18. Four specific pixel spot patterns are shown for the center pixel, the smallest RMS spot size, a moderately high RMS spot size, and the worst RMS spot size. In general, the spot shapes for a given RMS are very similar. For the Blue channel, the RMS spot sizes have less variation from pixel to pixel, although the mean RMS spot size is larger. Finally, the Strehl ratio of the entire system was calculated in the Blue and Red channels, varying from 99.2% in the worst case in the Red channel to >99.9% for the best case in both channels. It is interesting to note that the Blue channel has an uniform RMS and Strehl ratio regardless of placement on the detector and the Red Channel has more variation along the detector.

4.2. Diffraction Analysis

4.2.1. Scalar

As discussed in §3.1, the slicer mirrors, 3 × 15 mm rectangular, or 20 wavelengths at 150 μm, cut significantly into the Airy disk of the telescope (Figure 19), causing strong diffraction from that point on. As diffraction effects play a major role in the optical performance of FIFI LS, a scalar diffraction analysis of the system was performed, numerically solving the problem using the propagation of waves between the optical components that are described using true scalar wave propagation, instead of the more commonly found Gaussian beam approximation. Detailed analysis was performed of both the Red and Blue channels, but as they are similar only the Red channel diffraction effects are discussed. All optics in front of the slicer assembly, including telescope, are assumed to be adequately oversized that no diffraction losses occur before the slicer mirrors.

The consequence of the slicer mirror cutting into the Airy pattern is shown for the three sets of slicer assembly mirrors (Figure 19). This causes a significant diffraction effect on the capture mirror— compare the ray trace pattern in Figure 10 to Figure 19. There are obvious sidelobes from the sharp edge (the pupil is effectively the Fourier Transform of the sampled focus) of the slicer mirror where one would not expect the beam in the simple ray trace. At this wavelength, the slicer mirror already cuts out some of the high frequency Fourier components along the x-direction, leading to a dip in the peak of the intensity on the capture mirror. The capture mirror was made large enough to capture as much of the diffraction side-lobes as possible (15 × 30 mm rectangular), and in Figure 19 one can see two sidelobes are recovered. Nonetheless, even with the oversized mirror, some of the higher order Fourier terms are still missing, causing a small depression in the peak of the intensity on the slit mirrors (4 × 8 mm rectangular). This is only necessarily true at this wavelength. At other wavelengths, either negative or positive power is added at higher order, causing different peak structure.

The largest consequence of the diffraction in the slicer mirror assembly is that the collimator mirrors in the spectrometer must be large enough to keep as much of the sidelobes as possible, requiring very large biconic mirrors. One of the most important instrumental effects of the diffraction is the elongation of the pupil on the gratings. Since the slicer mirrors cause an effective spreading in the spectral dimension, the effective resolution of the spectrometer is increased— more lines of the grating are illuminated and the amplitude of the illumination varies across the grating, again compare Figure 14 to 20. Note that the peak features are dependent upon the wavelength, implying it is a function of the sampling of the sidelobes, and that at the longest wavelength the grating is over-illuminated. Finally,

the result of all the combined diffraction analysis effects at the detector pixel is seen at the bottom of Figure 20. The pixel size well samples the diffraction pattern on the detector.

4.2.2. Vector

The scalar diffraction analysis has an obvious deficiency: a real electromagnetic field can not be accurately described as a simple scalar field. For the correct treatment of diffraction, the complete set of 3-dimensional vector functions must be followed through the optical path. This may reveal important effects that impact the scalar estimation, such as polarization dependent diffraction. To investigate differences between the results from the GLAD program and the complete solution to the vector equations (Smythe 1947), the diffraction effects of the first two slicer mirrors were compared (also see Raab 2002, 2003). In Figure 21, the result for the numerically solved diffraction vectorial equation is shown. The intensity on both the slicer and capture mirrors are qualitatively the same as the scalar approximation, even down to small variations in the overall shape. The polarization effect on the slicer mirror is merely a numerical resolution problem since it is the original telescope diffraction pattern (symmetric diffraction should not have polarization differences), but the polarization variation is somewhat noticeable on the capture mirror, but still negligible. Thus, the simpler scalar approximation well describes the effects of the FIFI LS optics.

4.3. Throughput

The diffraction analysis is used to estimate light loss from the image slicer assembly and its relative effect on the overall throughput of the spectrometer. Figure 22 illustrates the integrated light loss from diffraction after each mirror surface, assuming 100% light at the slicer mirrors. The largest losses of light are from the capture mirrors and the first collimator mirror in both channels. In both channels, the higher order sidelobes are lost due to the physical size of the mirrors, although in the Blue channel the diffraction effects of the collimators are less important. Nonetheless, the contribution to light loss or throughput of the spectrometer from diffraction and vignetting in FIFI LS are minimal (<6%) at most operating wavelengths, although it can be as large as 28.5% at the extreme range of 210 μm. The two largest contributions of the overall FIFI LS throughput are the detectors (quantum efficency of $\sim$30%) and the gratings (Figure 7 median efficency of $\sim$70%). The final FIFI LS design is estimated to have a system efficency of $\sim$10%, which is large for a far-infrared spectrometer.

4.4. Spectral Resolution

Arguably, the most important aspect of the diffraction estimation is the increase and modification of the pupil on the grating, directly influencing the number of grating lines illuminated and the final overall spectral resolution (Figure 23). The diffraction effect was calculated as an effective aperture of the grating at various tilts, corresponding to the wavelength. Additionally, as in the real system, the pixel sampling effects were taken into consideration for the spectral response. The pixel sampling leads to a slight widening of the spectral response (Figure 23). The spectral resolving power is defined as the FWHM of the spectral response function, which varies strongly with observing wavelength.

4.5. Estimated FIFI LS Performance

FIFI LS will operate such that the detectors are always in the regime of Background Limited Infrared Photodetectors, or BLIP. With this basis and some reasonable assumptions about the emissivity of the telescope, optics, and baffling, the efficiency of the detectors as a function of wavelength, and the results of the throughput of the diffraction analysis in this paper, the overall performance of FIFI LS can be reliably estimated. Using the noise equivalent power of the the photons contributed from each item in the optical path as described by Bose-Einstein statistics (e.g. Lugten 1987), the overall instrumental sensitivity (Figure 24) to within 25% estimated error is derived.

5. Conclusion

As has been shown in other wavelength bands, integral field instrumentation can provide a very useful tool to probe many astronomical problems. However until recently, far-infrared integral field instruments were not technically feasible due to the small size of the detector arrays. Now with the new, large format detectors, the first integral field instrument has been designed in the far-infrared using a novel design with a reflective slicer mirror assembly. In addition, the instrument is designed to have high observing efficiency for extragalactic sources via the integral field optics, the simultaneous, dual-channel design, and by using moderate resolution reflective gratings. With these advantages and the increase in spatial resolution and sensitivity on SOFIA, FIFI LS will provide a major step forward for far-infrared spectroscopy.

The core of the FIFI LS design is a slicer mirror assembly that re-arranges the 2-dimensional field of view into a 1-dimensional pseudo-slit. The slit can then be dispersed

with a standard long-slit spectrometer. In this arrangement, the field of view is spread out horizontal along the detector, while the spectral information is dispersed vertically. However, this design causes significant diffraction due to the Airy disk of the telescope being cut by the small slicer mirrors. The main diffraction effects are a small loss of light and an enlarged illumination pattern on the grating. However with careful design, the loss of light can be decreased to less than 6% for most observations by properly oversizing the optical components. (A good rule of thumb was to double the size of the mirrors needed for ray-tracing, especially for pupil-equivalent elements.) Finally, the performance of the FIFI LS system was estimated. FIFI LS is expected to be $\sim$3 times more sensitive for point sources than LWS on ISO at 160 μm and with more 25 times the number of spatial pixels, higher spatial resolution, and higher spectral resolution (for LWS in the grating mode). FIFI LS is not compared to SIRTF as there is no real spectroscopic instruments in the FIFI LS wavelength regime. PACS, onboard Herschel, will have the advantages of a cooled and larger telescope, estimated to be about 6 times more sensitivity than for FIFI LS.

Unlike space borne missions, it will be possible to have future upgrades to FIFI LS. For example, enlarging the field of view to 7×7 pixels, requiring a larger detector, or adding a shorter wavelength detector (e.g. perhaps Si:Sb). However, because of the difficult nature of stressing Ge:Ga detectors for the Red channel (Hönle et al. 2004), the maximum foreseeable array size is being reached. Arbitrarily more pixel stacks can be added, but the stressing mechanisms required for long wavelength sensitivity of Ge:Ga can only be increased by at most factors of 2. One possible future solution, which would allow larger format arrays, would be the use of Ga:As BIB detectors (Poglitsch et al. 2003).

We especially thank the FIFI LS team and Reinhard Genzel for supporting this project. In addition, we thank the referee Alfred Krabbe for his comments.

REFERENCES

Ade, P.A.R. 2003, private communication

Arribas, C., Carter, D., Cavaller, L., del Burgo, C., Edwards, R., Fuentes, F.J., Garcia, A.A., Herreros, J.M., Jones, L.R., Mediavilla, E., Pi, M., Pollacco, D., Rasilla, J.L., Rees, P.C., & Sosa, N.A. 1998, Proc. SPIE 3354, 1998

Bacon, R., Adam, G., Baranne, A., Courtès, G., Dubet, D., Dubois, J.P., Emsellem, E.,

Ferruit, P., Georgelin, Y., Monnet, G., Pécontal, E., Rousset, A., & Sayéde, F. 1995, A&AS, 113, 347

Bacon, R., Copin, Y., Monnet, G., Miller, B.W., Allington-Smith, J.R., Bureau, M., Carollo, C.M., Davies, R.L., Emsellem, E., Kuntschner, H., Peletier, R.F., Verolme, E.K., & de Zeeuw, P.T. 2001, MNRAS, 326, 23

Content, R. 1997, Proc. SPIE, 2871, 1284

Courtès, G. 1982, Instrumentation for Astronomy with Large Optical Telescopes, ed. C.M. Humphries (Reidel), 123

Eisenhauer, F., Tecza, M., Mengel, S., Thatte, N., Röhrle, C., Bickert, K., & Schreiber, J. 2000, Proc. SPIE, 4008, 676

Erickson, E.F. 1995, Space Sci. Rev., 74, 9

Geis, N., Poglitsch, A., Raab, W., Rosenthal, D., Kettenring, G., & Beeman, J.W. 1998, Proc. SPIE, 3354, 973

Goray 1995, Proc. SPIE, 2532, 427

Haynes, R., Lee, D., Allington-Smith, J.R., Content, R., Dodsworth, G., Lewis, I., Sharples, R., Turner, J., Webster, J., Done, C., & Peletier, R. 1999, PASP, 111, 1451

Heim, G.B., Henderson M.L., MacFeely K., McMahon T.J., Michika D., Pearson R.J., Rieke G.H., Schwenker J.P., Strecker D.W., Thompson C., Warden R.M., Wilson D.A., and Young, E.T. 1998, Proc. SPIE, 3356, 985

Hönle, R. et al. 2004 in preparation

Krabbe, A., & Röser, H.P. 1999, Reviews in Modern Astronomy 12, p.107

Larson, H.P. 1995, in Astronomical Society of the Pacific, Airborne Astronomy Symposium on the Galactic Ecosystem: From Gas to Stars to Dust, Volume 73 p 591-608 (SEE N96-13618 02-88)

Looney, L.W., Raab, W., Poglitsch, A., Geis, N., Rosenthal, D., Hoenle, R., Klein, R., Fumi, F., Genzel, R., & Henning, T. 2003, Proc. SPIE, 4857, 47

Looney, L.W., Geis, N., Genzel, R., Park, W-K., Poglitsch, A., Raab, W., Rosenthal, D., Urban, A., Henning, T. 2000, Proc. SPIE, 4014, 14

Lugten, J.B. 1987, Ph.D. Thesis, University of California, Berkeley

Tecza, M., Thatte, N., Eisenhauer, F., Mengel, S., Röhrle, & Bickert, K. 2000, Proc. SPIE, 4008, 1344

Pilbratt, G.L. 2003, Proc. SPIE, 4850, 586

Poglitsch, A., Beeman, J.W., Geis, N., Genzel, R., Haller, E.E., Jackson, J., Rumitz, M., Stacey, G.J., & Townes, C.H. 1991, Int. J. IT & Millimeter Waves, 12, p.859

Poglitsch, A., Katterloher, R.O. Hönle, R., Beeman J.W., Haller E.E., Richter H., Grözinger U., Haegel N.M., & Krabbe A. 2003, Proc. SPIE, 4855, in print

Poglitsch, A., Waelkens, C, & Geis, N 2003, Proc. SPIE, 4850, 662

Raab, W. 2002, Ph.D. Thesis, Ludwig-Maximilian University, Munich, Germany

Raab, W., Looney, L.W., Poglitsch, A., Geis, N., Hönle, R., Rosenthal, D., & Genzel, R. 2003, Proc. SPIE, 4857, 166

Rosenthal, D., Beeman, J.W., Geis, N., Looney, L.W., Poglitsch, A., Park, W.K., Raab, W., & Urban, A., 2000, Proc. SPIE, 4014, 156

Smythe, W.R. 1947, Phys. Rev., 72, 1066

Weitzel, L., Krabbe, A., Kroker, H., Thatte, N., Tacconi-Garman, L.E., Cameron, M., & Genzel, R. 1996, A&AS, 199, 531

Vanderriest, C. 1980, PASP, 92, 858

This preprint was prepared with the AAS LaTeX macros v5.0.

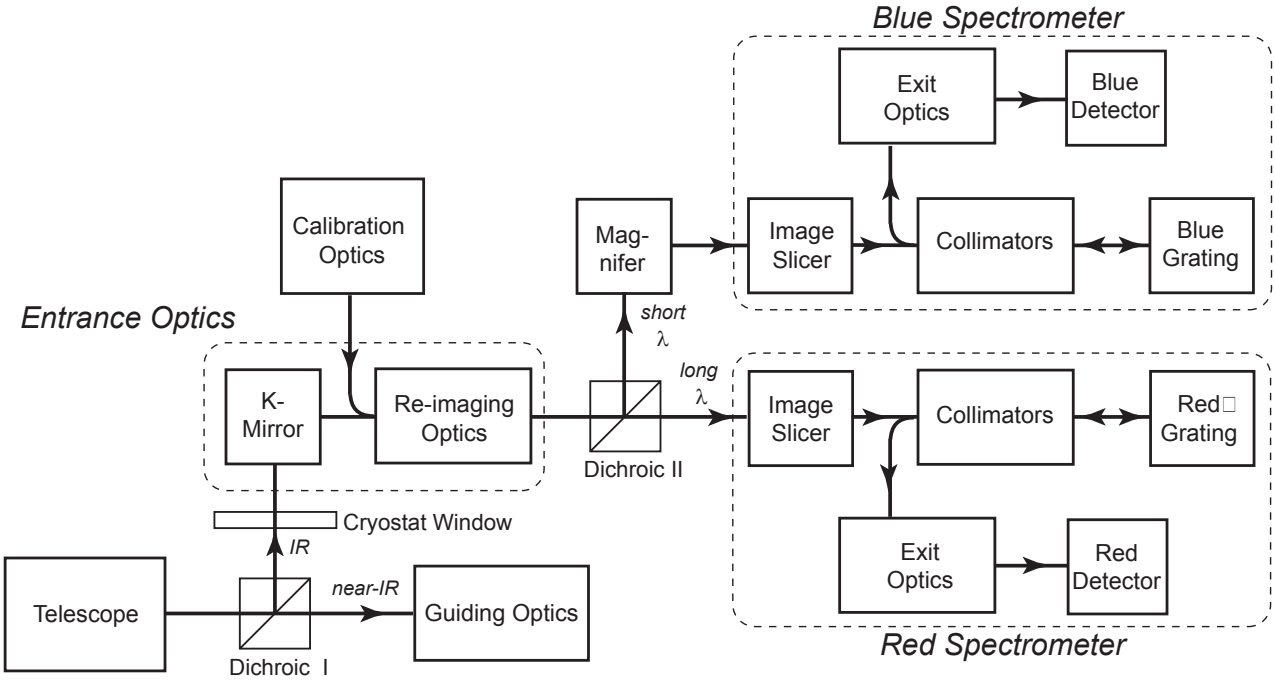

Fig. 1.— A simplified schematic overview of the FIFI LS optics in block format. The calibration optics (including the graybody source) can be switched into the path via a flip-mirror. The spectrometer is near-Littrow mounted, so the collimator mirrors are dual-path optics.

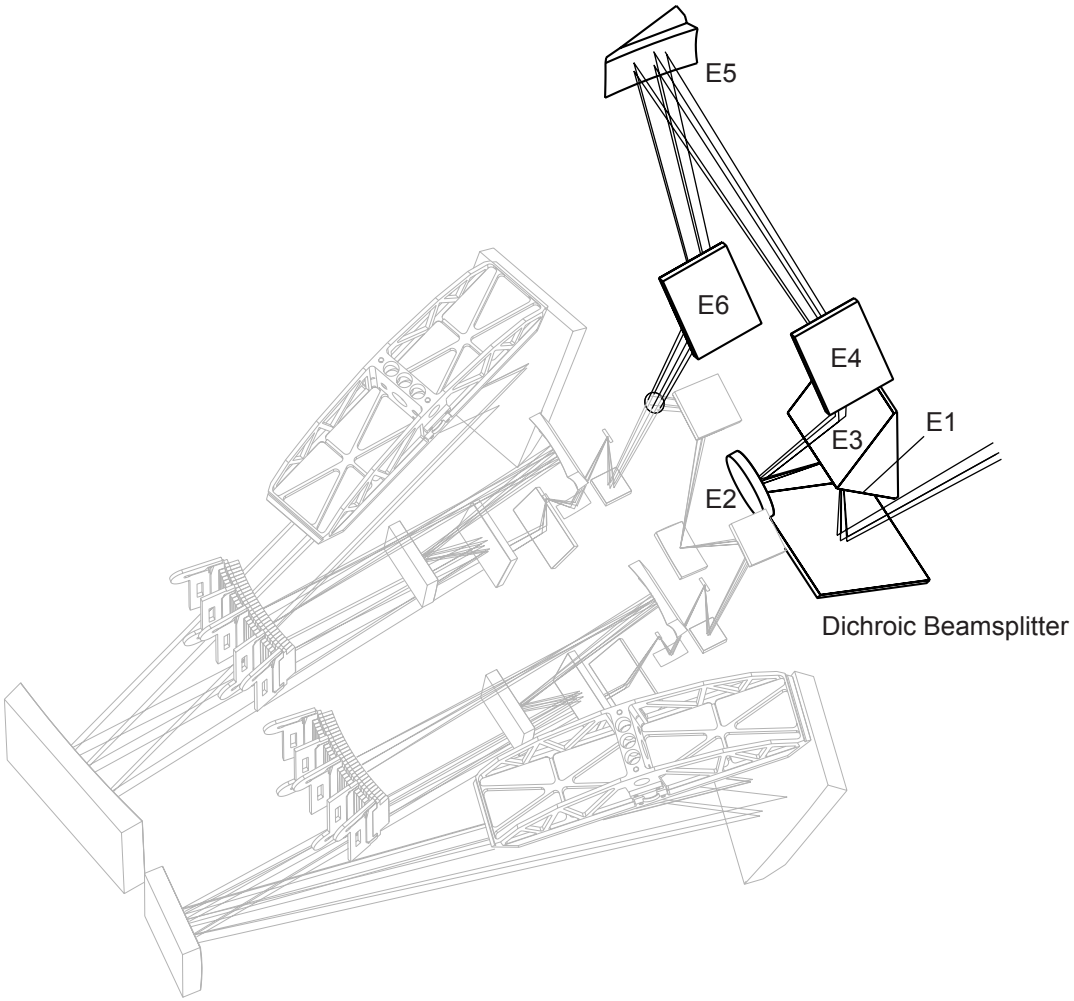

Fig. 2.— The optics of the FIFI LS design with the entrance optics highlighted and labeled (calibration path not shown for clarity).

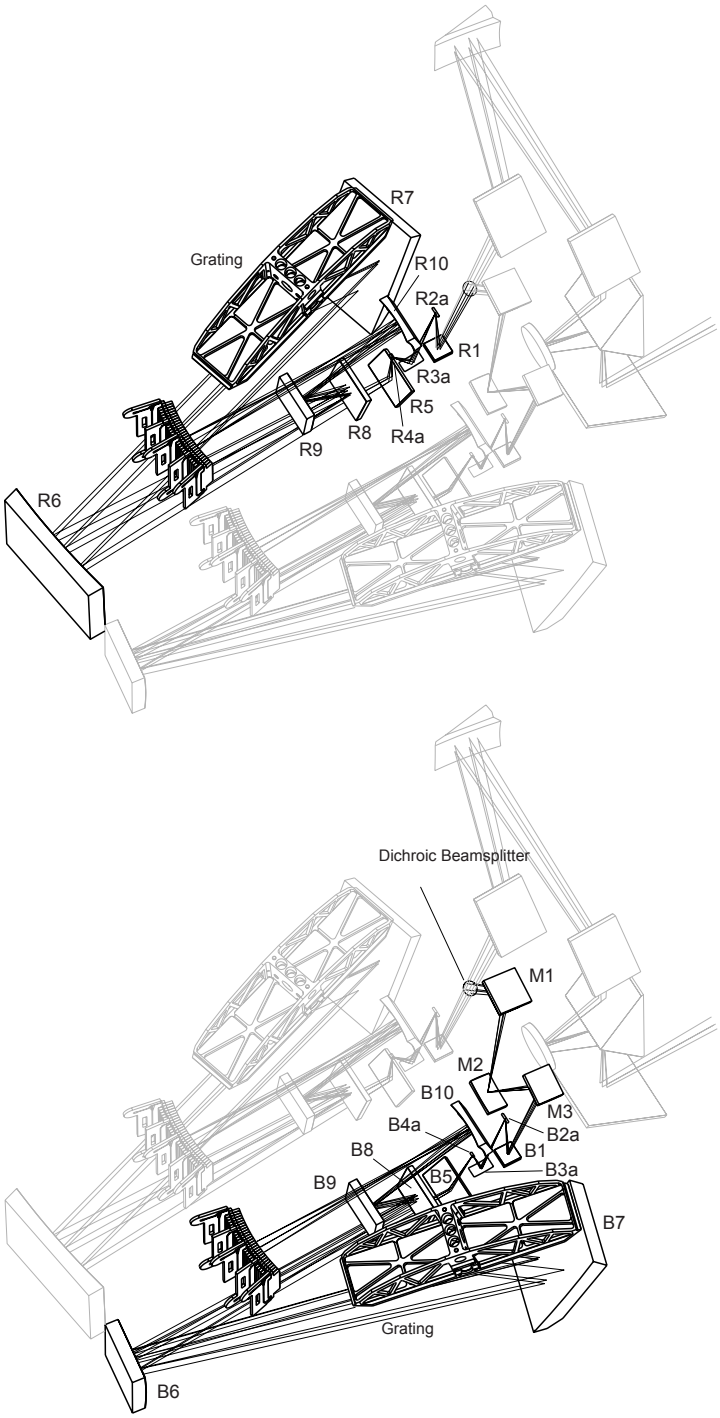

Fig. 3.— The FIFI LS optical system with the Red (upper) and Blue (lower) spectrometers highlighted.

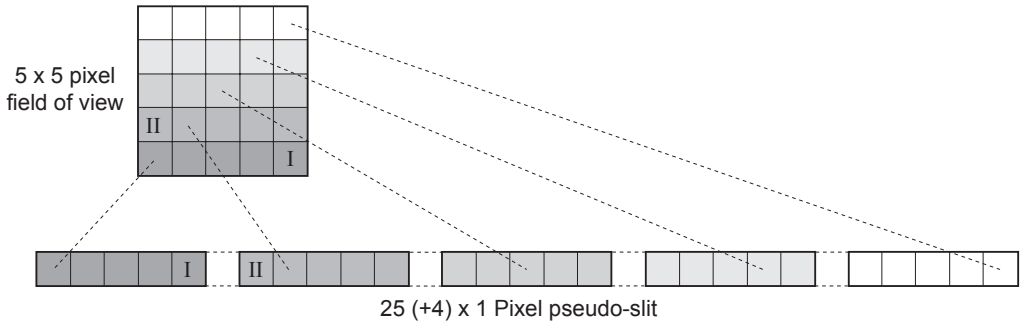

Fig. 4.— A detail showing the basic design premise for the FIFI LS image slicer. The optics must slice the rows of the 5×5 pixel field-of-view into a 25×1 pixel pseudo-slit. The gaps in the slit are added to reduce cross-talk between nonadjacent field pixels (e.g. pixels I and II).

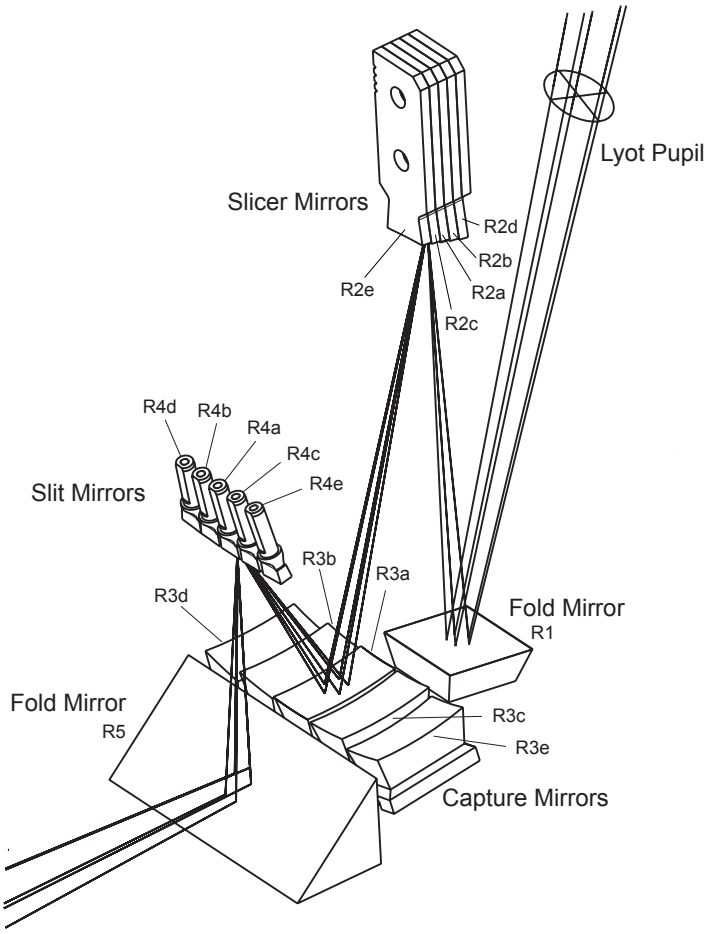

Fig. 5.— Close up view of the slicer assembly mirror components for the Red channel with only the rays of the central slice shown. The Blue channel is similar.

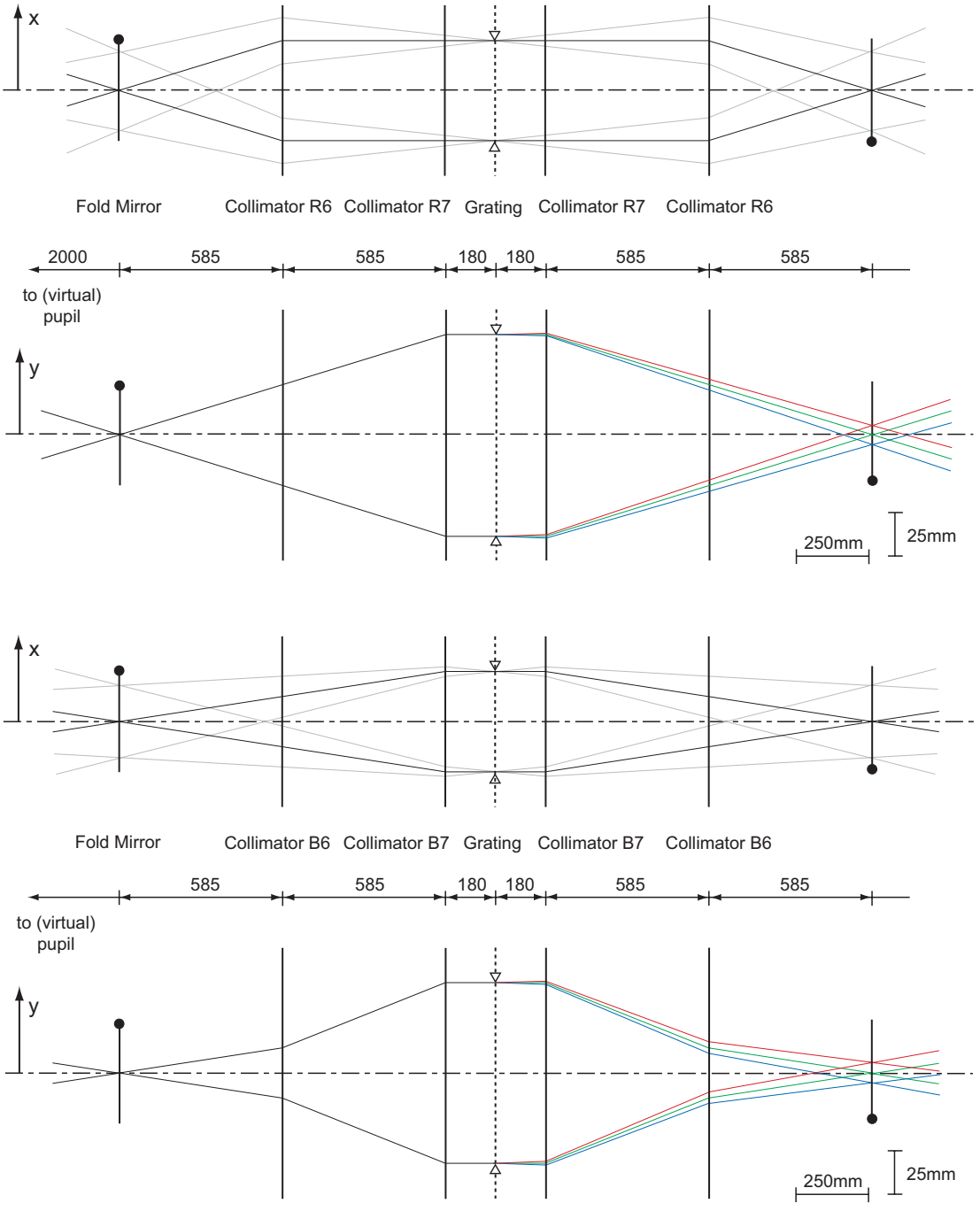

Fig. 6.— A simple schematic of the Red (top) and Blue (bottom) spectrometer design in FIFI LS. For ease of display and concept, the mirrors are shown as lenses. The x-axis is the cross-dispersion direction (along the slice) and the y-axis is along the spectral dispersion direction (perpendicular to the slice).

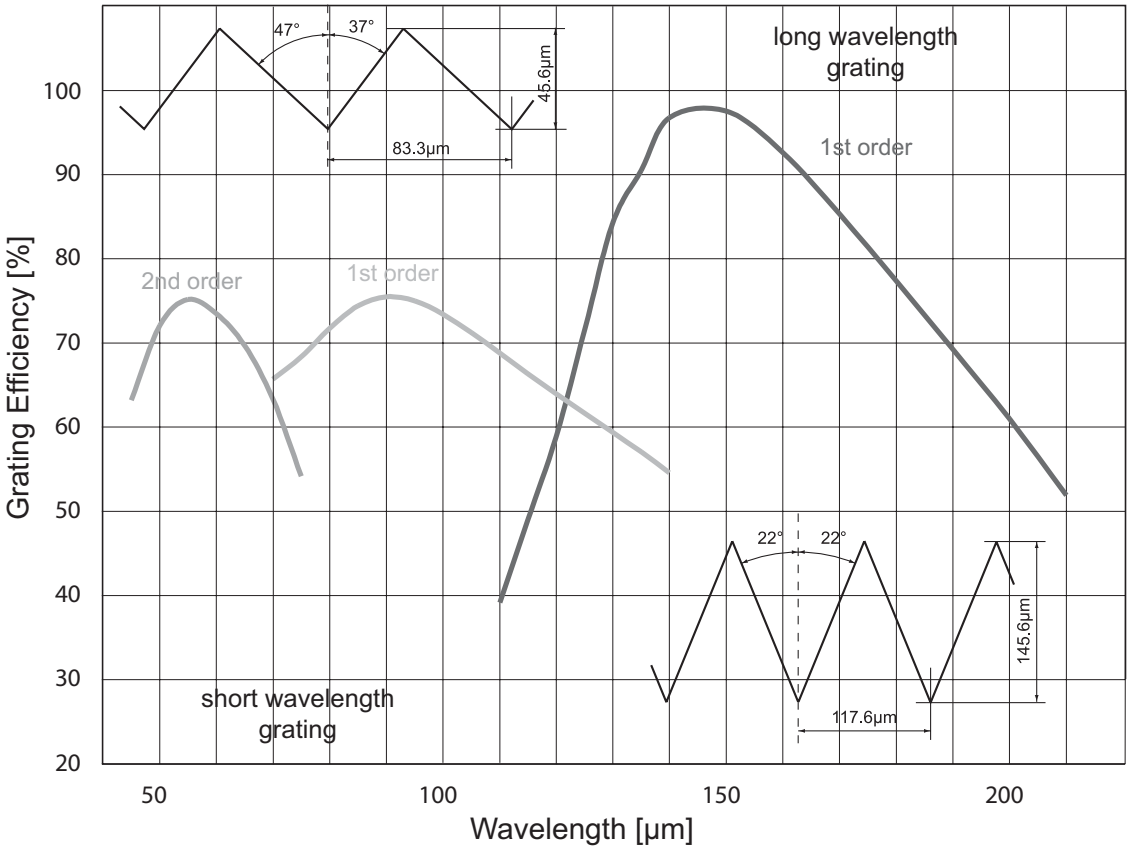

Fig. 7.— Overall efficiency of the Red and Blue gratings. The inserts show the grating profile of each grating. Grating profiles are not to scale. Note that the Red and Blue spectral channels can be separated at either 105 or 130 μm.

Table 1. FIFI LS filter list

Nomenclature	Position	Type	Reflectance [μm]	Transmission [μm]	Size [mm]
L2	Lyot Stop	highpass	···	40 - >210	30 Ø
D1	Dichroic	reflect	41 - 105	105 - 220	30 Ø
D2	Dichroic	reflect	60 - 130	130 - 220	30 Ø
R01	Red Pupil	highpass	···	100 - >220	15 Ø
B01-A	Blue Pupil	bandpass	···	70 - 130	15 Ø
B01-B	Blue Pupil	bandpass	···	70 - 130	15 Ø
B02-A	Blue Pupil	bandpass	···	42 - 72	15 Ø
B02-B	Blue Pupil	bandpass	···	42 - 72	15 Ø
RAL	Red Detector	highpass	···	100 - >220	60×105
BAL	Blue Detector	highpass	···	42 - >130	60×105

Note. — B01 and B02 consist of two filters each– a low pass and high pass filter.

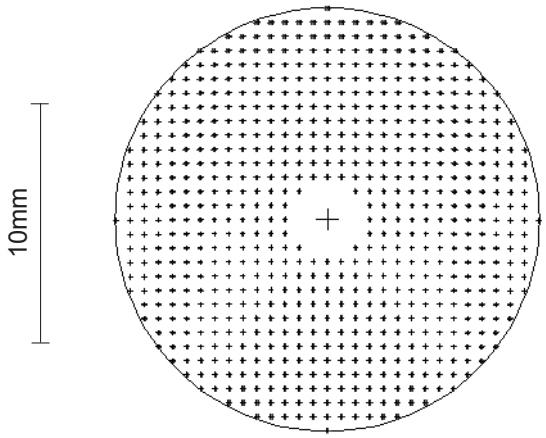

Fig. 8.— The entrance pupil for the slicer, 17.6 mm in diameter.

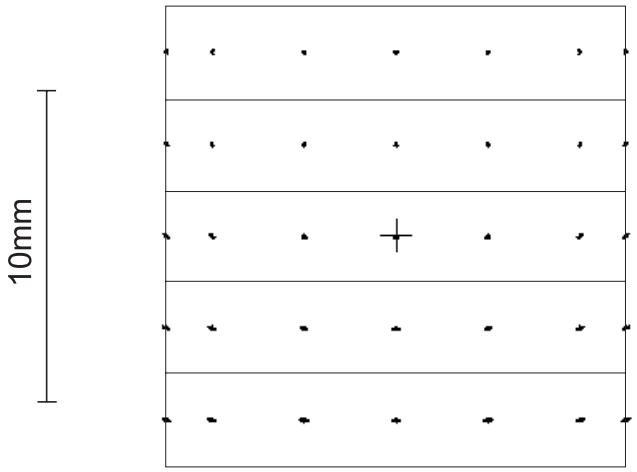

Fig. 9.— Simulation of the SOFIA telescope re-imaged focus on the slicer mirror stack in projection.

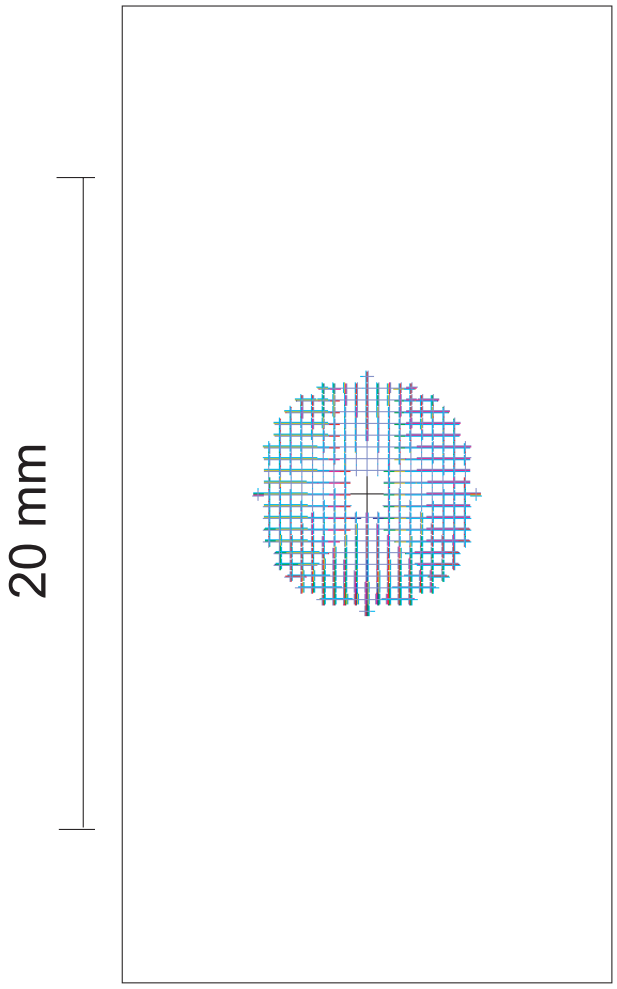

Fig. 10.— Quality of pupil on capture mirrors for the central slice.

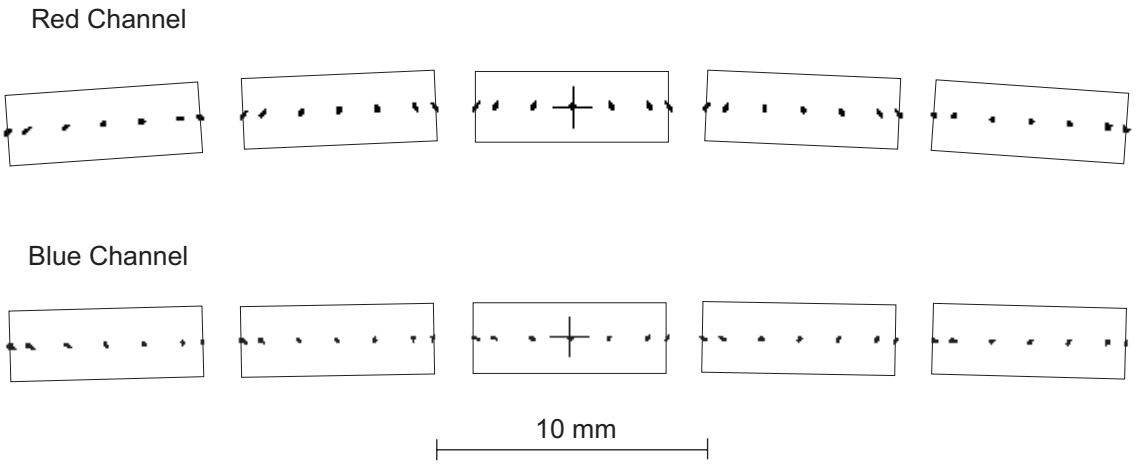

Fig. 11.— Simulation of the SOFIA telescope re-imaged focus on the slit mirrors. This is exactly equivalent to the entry slit of a long-slit spectrometer.

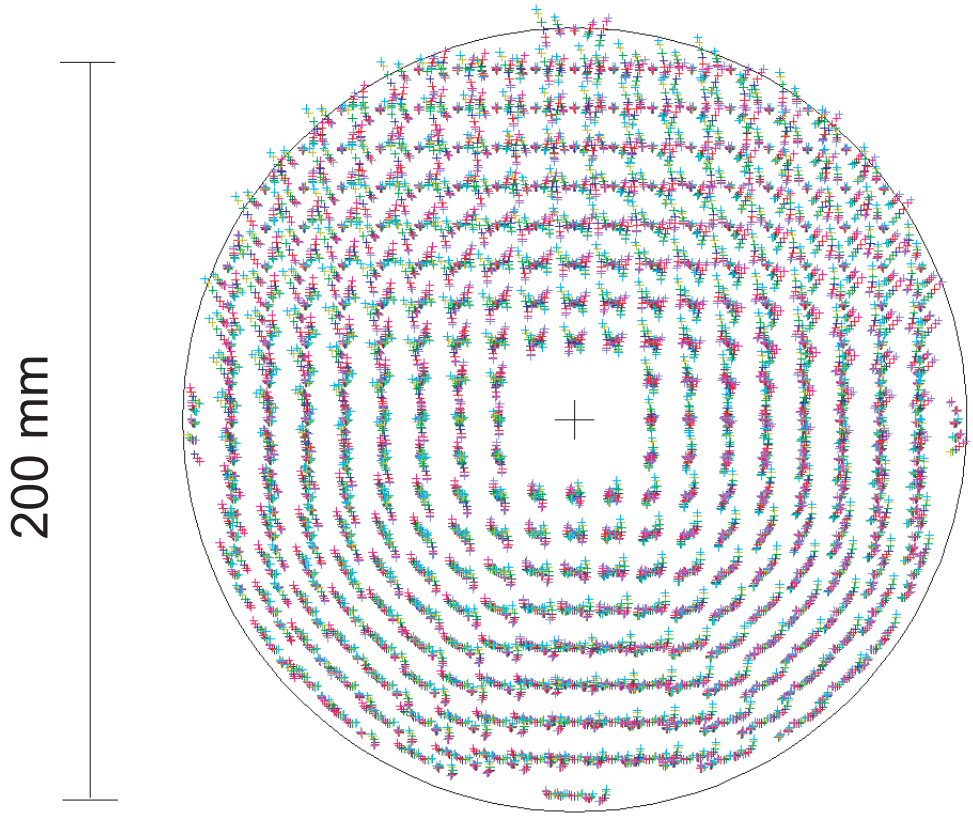

Fig. 12.— Recombined virtual pupil of the 5 slices as imaged by the slit mirrors.

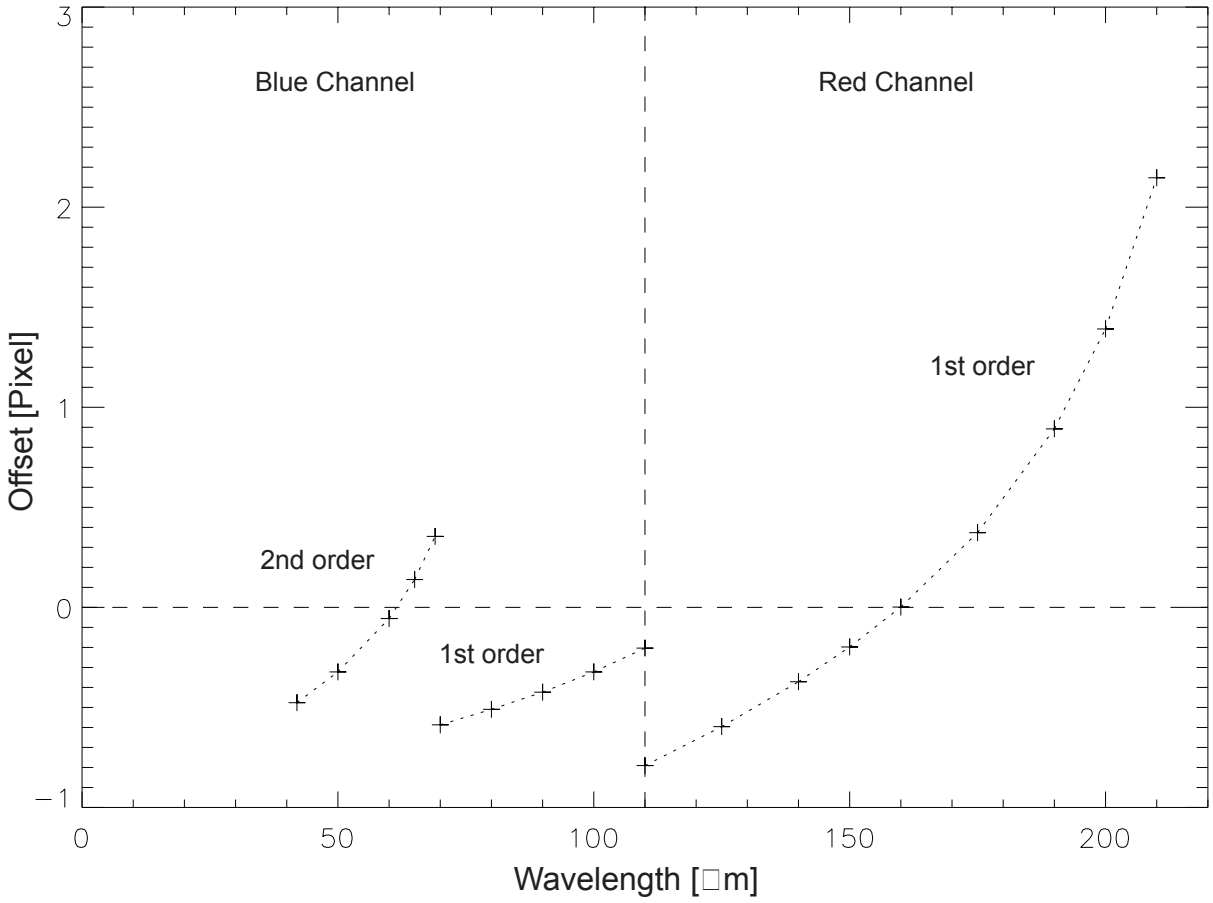

Fig. 13.— The overall "smile" of the system optimized to reduce grating smile. The maximal deviation from a straight slit is given in pixels as a function of wavelength. This is the residual after combining spectrometer "smile" and slicer system "frown".

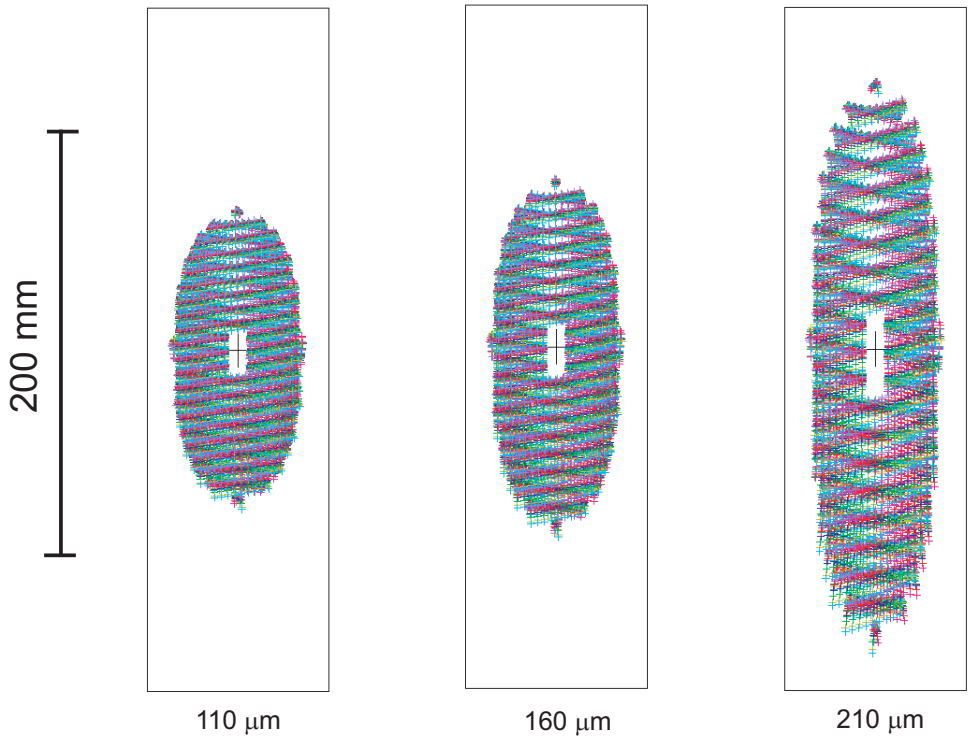

Fig. 14.— The ray-traced anamorphic pupil on the grating at three wavelengths in the Red Channel.

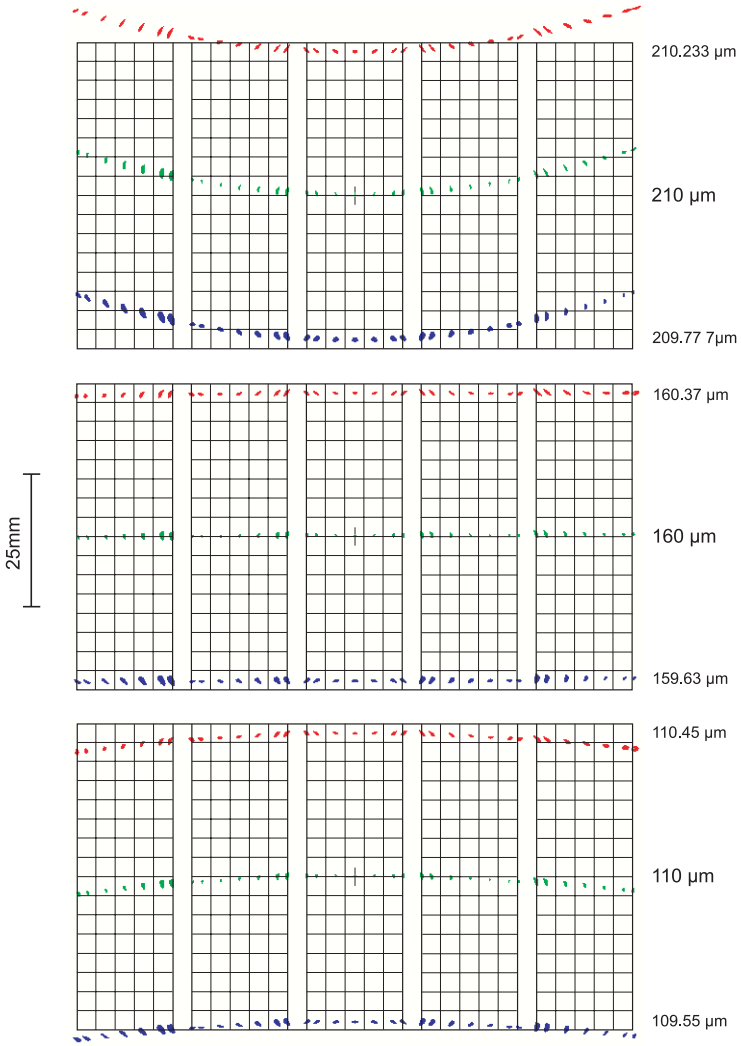

Fig. 15.— The final imaging of the dispersed beam at three wavelengths in the long wavelength Red channel.

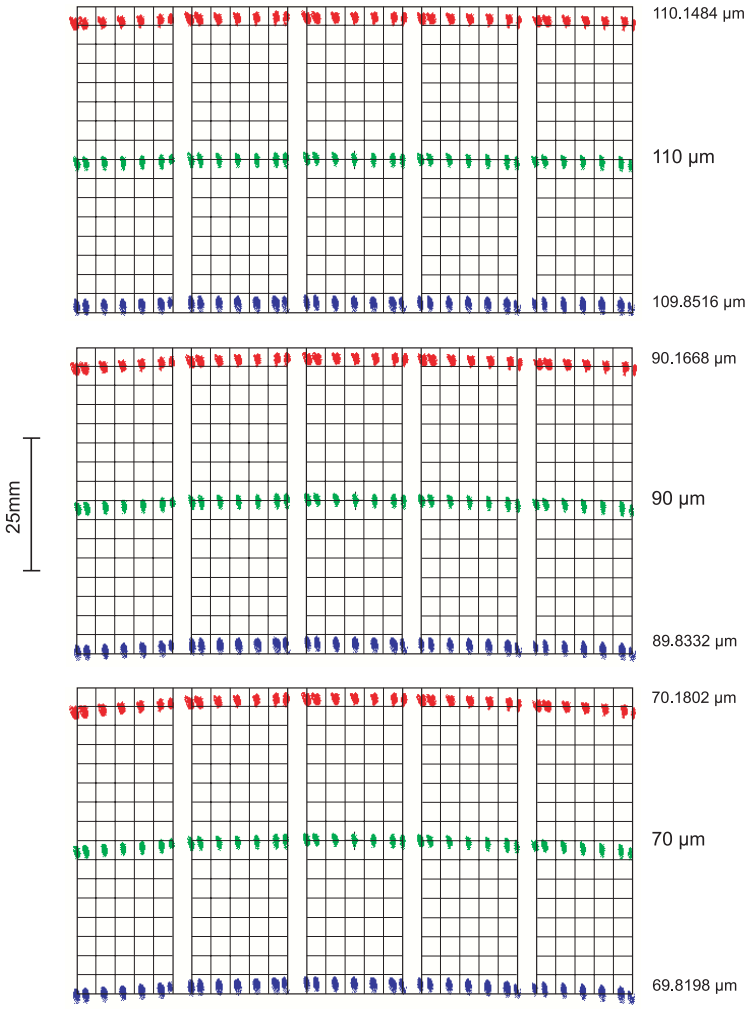

Fig. 16.— The final imaging of the dispersed beam at three wavelengths in the short wavelength Blue channel in first grating order.

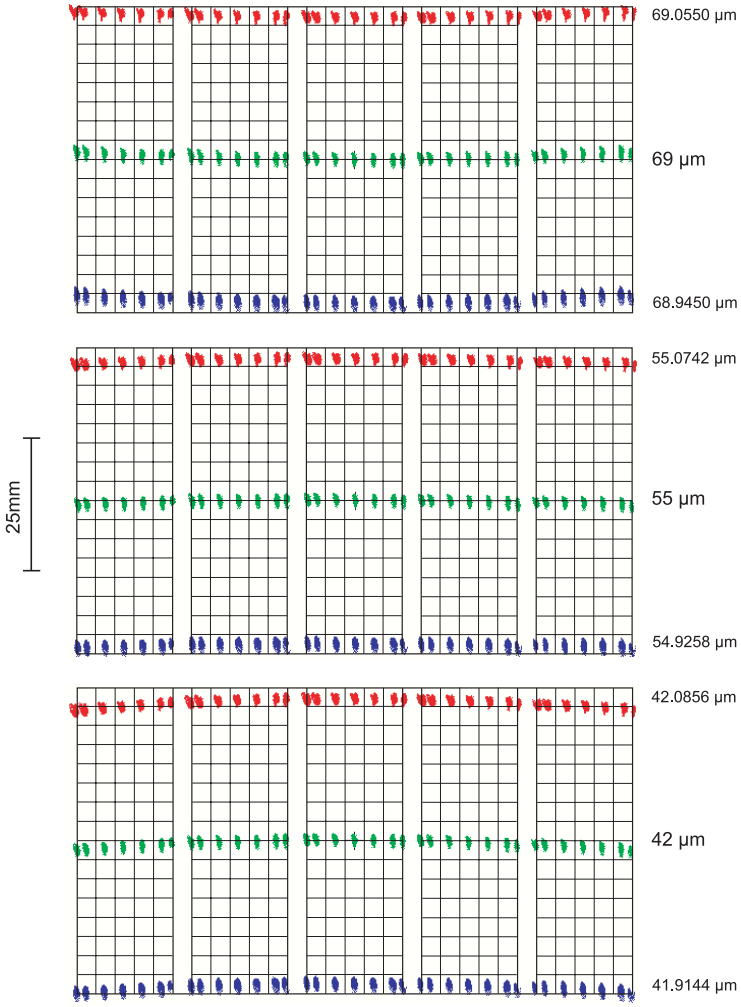

Fig. 17.— The final imaging of the dispersed beam at three wavelengths in the short wavelength Blue channel in second grating order.

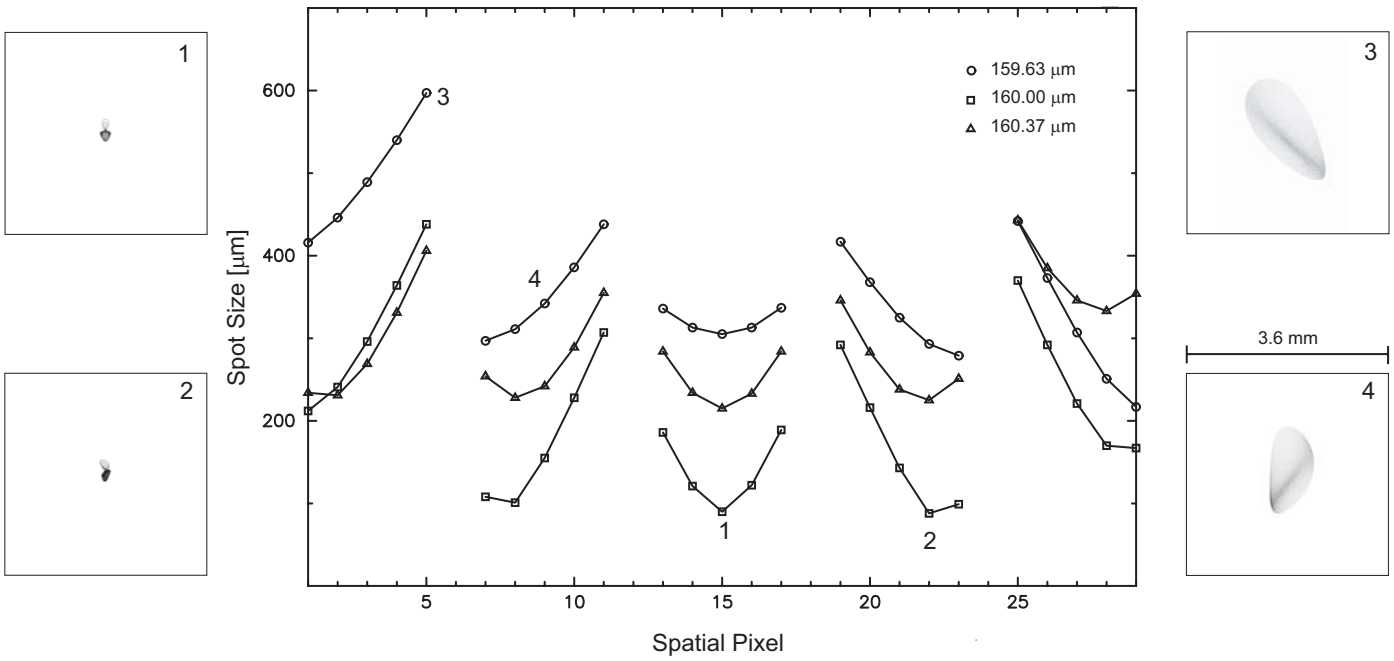

Fig. 18.— The RMS of the spot sizes on the red detector at 160 μm and the two dispersed wavelengths. Inserts show spot patterns for the center pixel, the smallest RMS pixel, a pixel with moderate RMS, and the pixel with the worst RMS, superimposed on detector pixel outlines, respectively. The Blue channel detector exhibits a more uniform spot size RMS over all pixels.

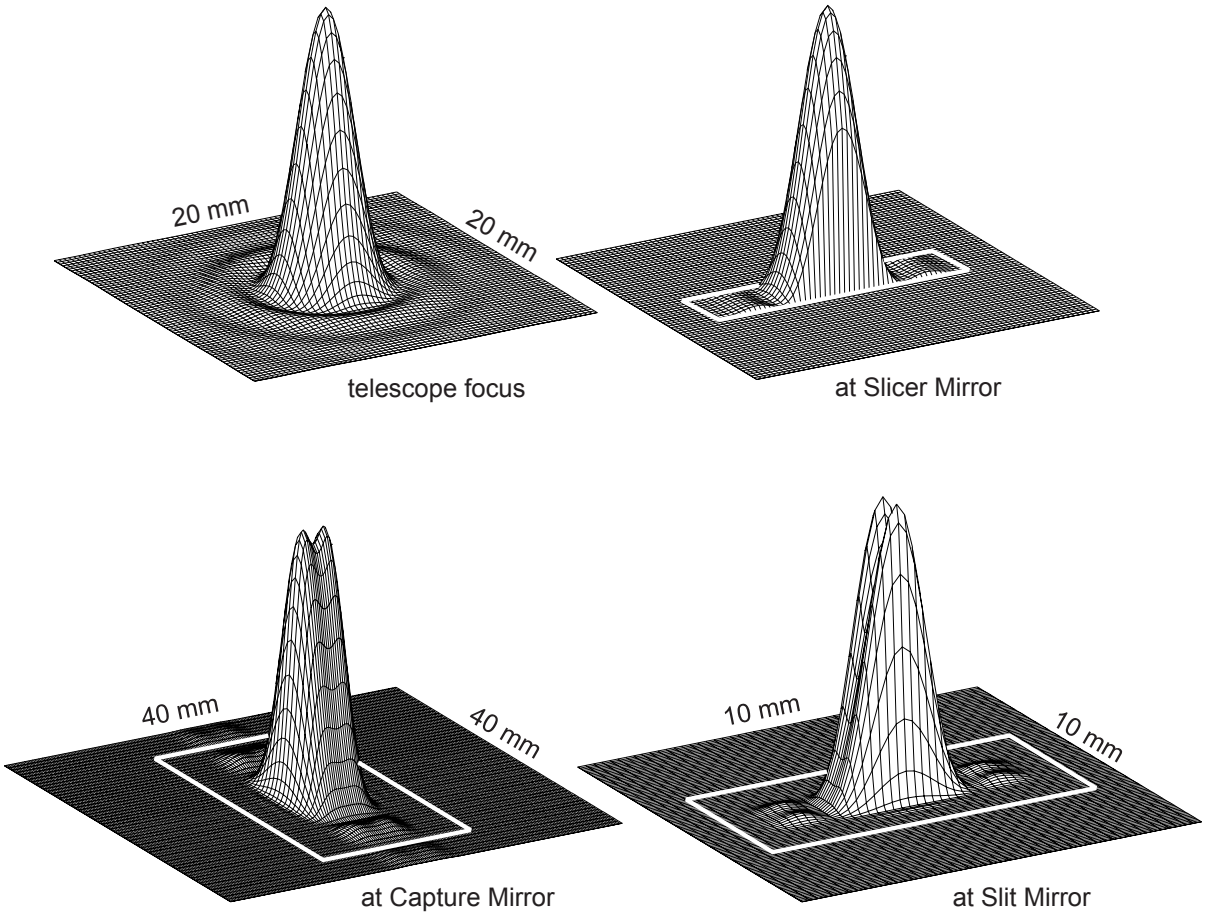

Fig. 19.— The diffraction effects of the three slicer mirrors for the central slice as estimated by using a scalar propagation method.

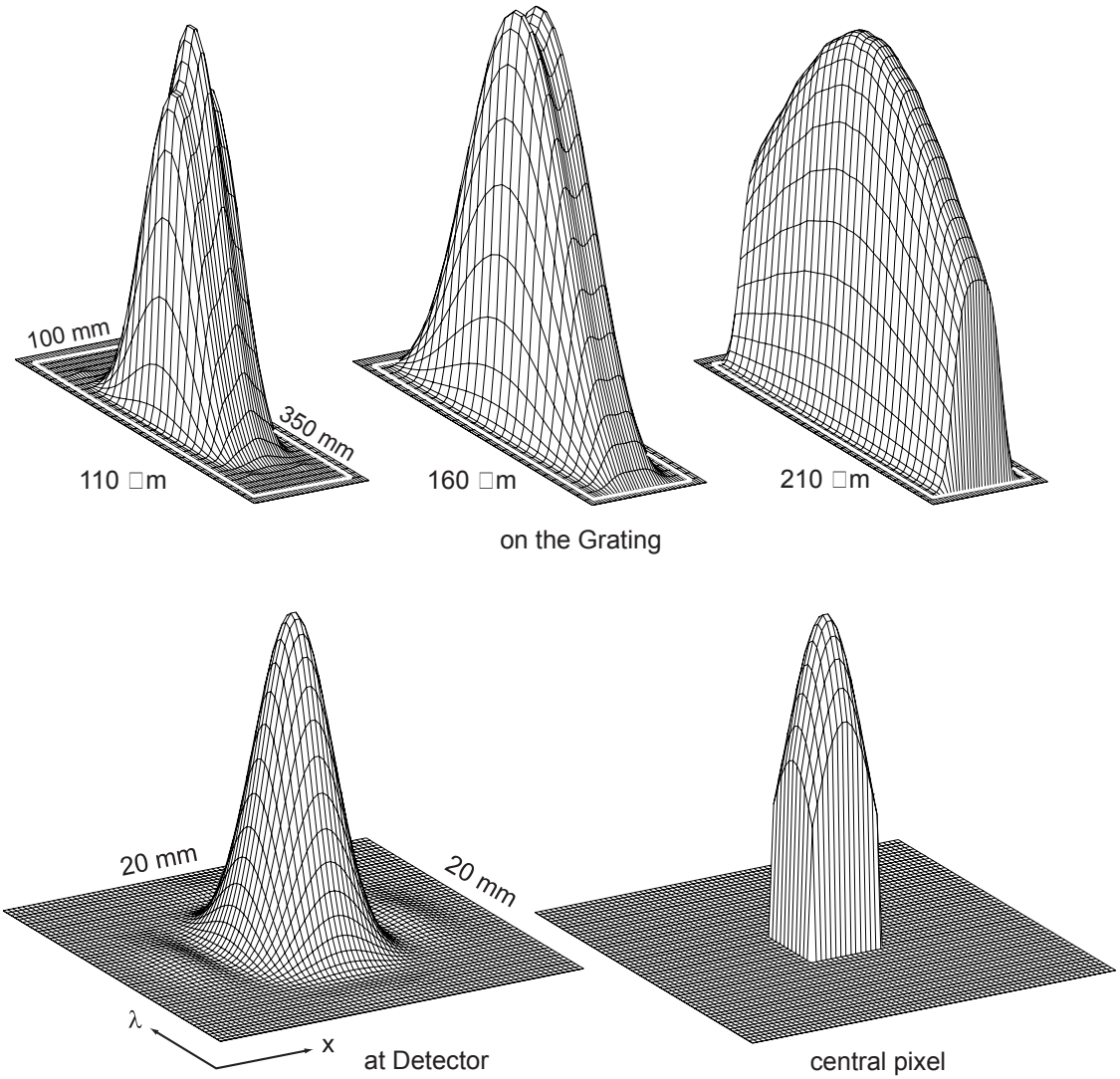

Fig. 20.— The diffraction effects arising from the slicer system on the grating at three wavelengths in the Red channel, and the "point spread function" for the central pixel of the detector at 160 μm.

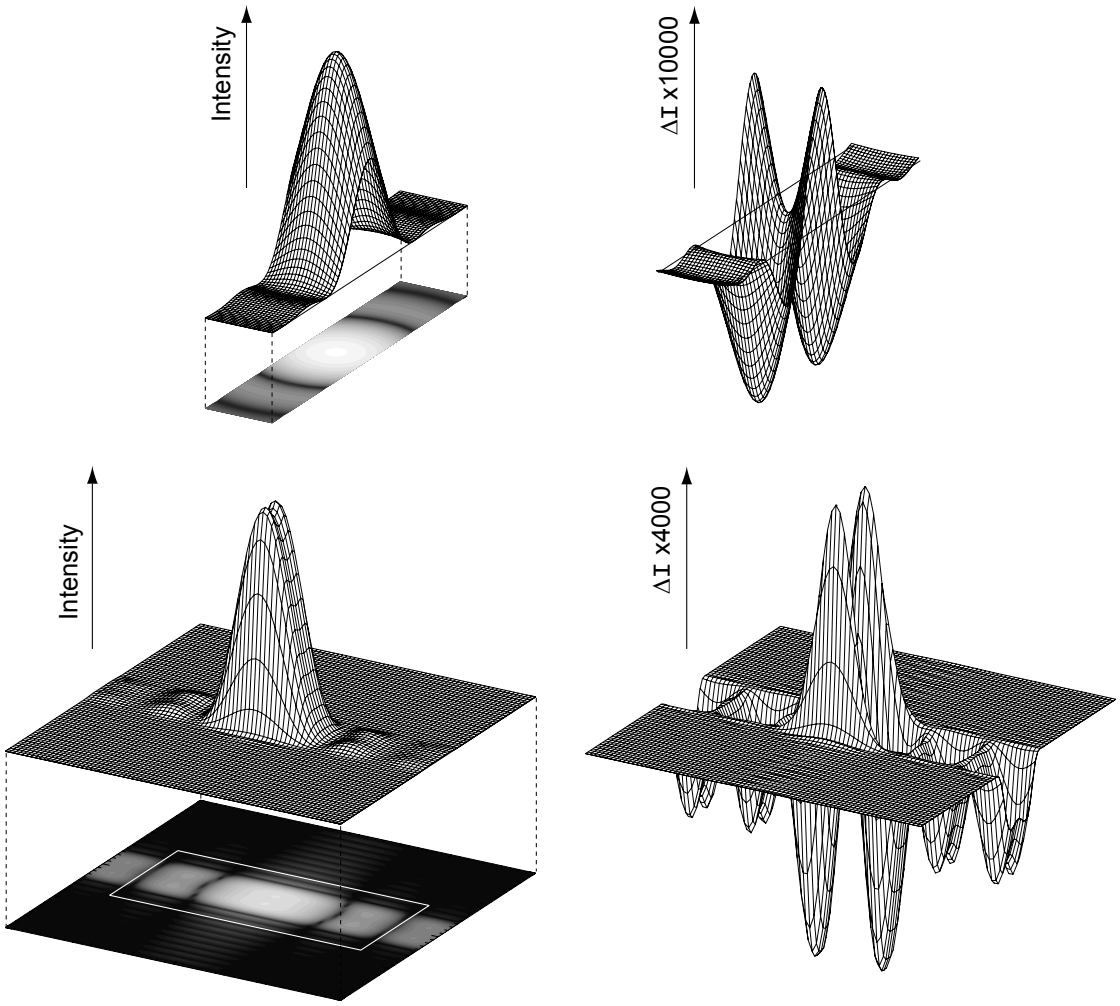

Fig. 21.— The diffraction effects as calculated using the complete vectorial solution to the fields. On the top is the diffraction pattern on the central Slicer Mirror and the difference between the two polarizations, multiplied by 1000 for clarity. On the bottom, the diffraction pattern on the central Capture Mirrors and the difference between the two polarizations, multiplied by 4000. The polarization difference on the top is most likely due to numerical rounding errors, and those on the bottom are real variations but insignificant in magnitude.

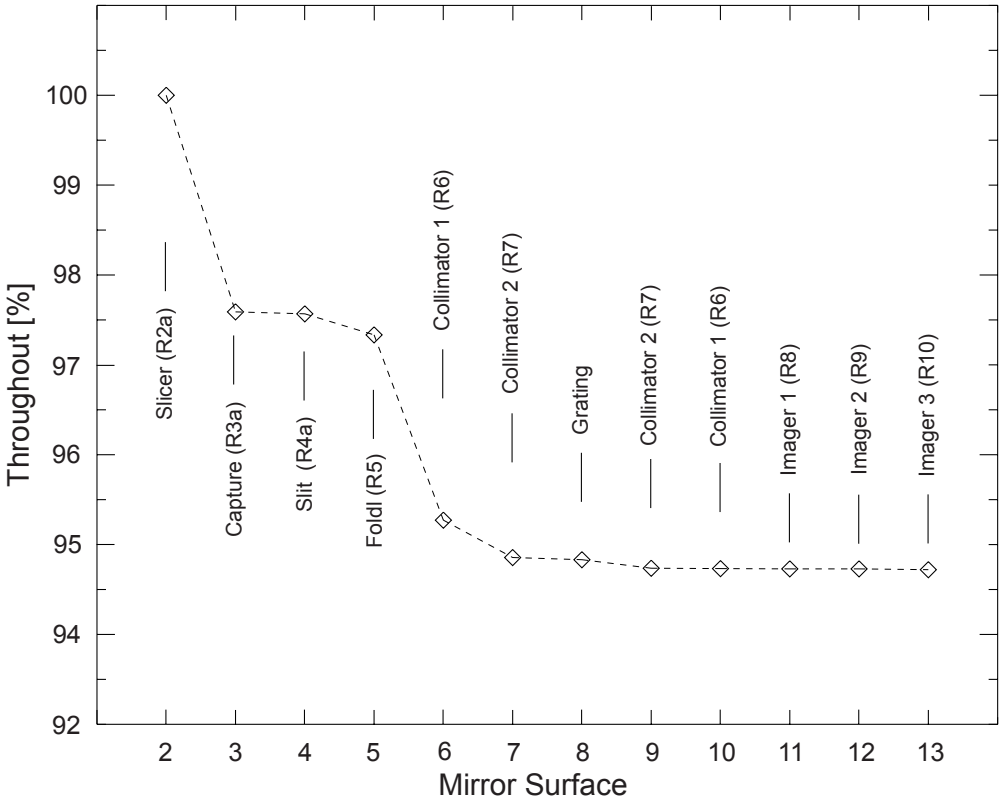

Fig. 22.— The light loss through the optics due to pure diffraction or vignetting effects at 160 μm. Note that the largest losses are from the capture and the first collimator mirrors.

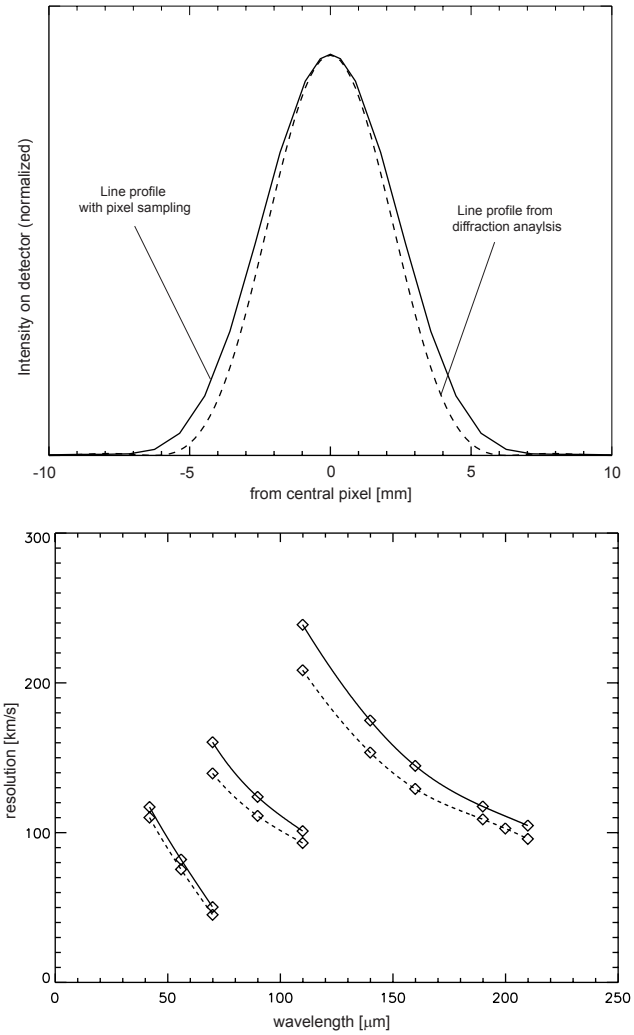

Fig. 23.— The modeled spectral resolution of FIFI LS: scalar diffraction analysis only (dashed), and with pixel sampling (solid).

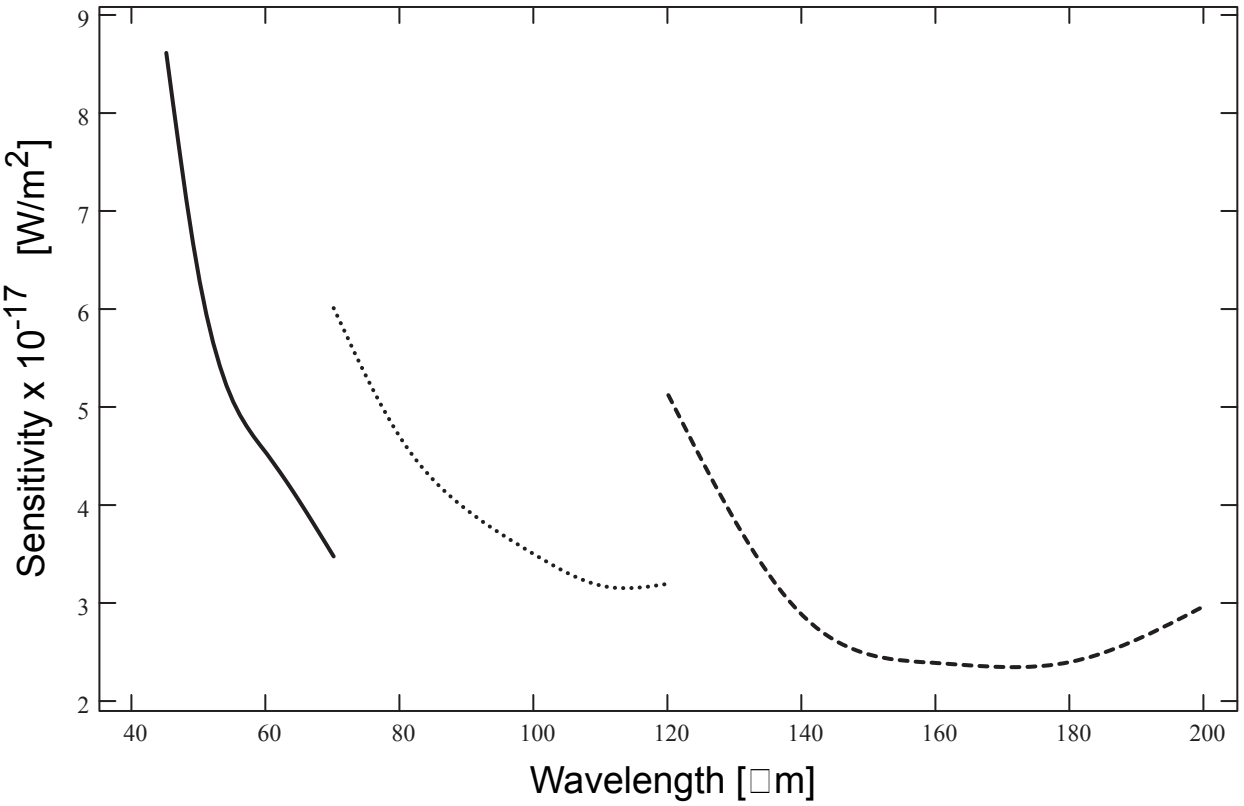

Fig. 24.— The expected sensitivity of FIFI LS for point-source detection (4σ in 15 minutes) as a function of wavelength, including pixel sampling effects, diffraction analysis, optical throughput (including the SOFIA telescope), pixel coupling efficency, and detector quantum efficency. The solid, dotted, and dashed lines are for the Blue channel first grating order, the Blue channel second grating order, and the Red channel first grating order, respectively.